Soft Matter

Double Membrane Formation in Heterogeneous Vesicles

Journal:	*Soft Matter*
Manuscript ID	SM-ART-06-2020-001167.R1
Article Type:	Paper
Date Submitted by the Author:	06-Aug-2020
Complete List of Authors:	Bolmatov, Dima; University of Tennessee, Department of Physics and Astronomy; Oak Ridge National Laboratory, Large Scale Structures Group, Neutron Scattering Division Carrillo, Jan Michael; Oak Ridge National Laboarotry, Sumpter, Bobby; Oak Ridge National Laboratory, Computer Science and Mathematics Division and Center for Nanophase Materials Sci Katsaras, John; Oak Ridge National Laboratory, Neutron Sciences Directorate Lavrentovich, Maxim; University of Tennessee, Department of Physics and Astronomy

Soft Matter

ARTICLE TYPE

Cite this: DOI: 00.0000/xxxxxxxxxx

Double Membrane Formation in Heterogeneous Vesicles

Dima Bolmatov,[*abc] Jan-Michael Y. Carrillo,[‡de] Bobby G. Sumpter,[de] John Katsaras,[abc] Maxim O. Lavrentovich[§bc]

Received Date
Accepted Date

DOI: 00.0000/xxxxxxxxxx

Lipids are capable of forming a variety of structures, including multi-lamellar vesicles. Layered lipid membranes are found in cell organelles, such as autophagosomes and mitochondria. Here, we present a mechanism for the formation of a double-walled vesicle (i.e., two lipid bilayers) from a unilamellar vesicle through the partitioning and phase separation of a small molecule. Using molecular dynamics simulations, we show that double membrane formation proceeds via a nucleation and growth process – i.e., after a critical concentration of the small molecules, a patch of double membrane nucleates and grows to cover the entire vesicle. We discuss the implications of this mechanism and theoretical approaches for understanding the evolution and formation of double membranes.

1 Introduction

Amphipathic molecules in bulk solution can self-assemble into a wide variety of stable structures, such as micelles, lamellae, vesicles (liposomes), and bicontinuous foamy phases. The study of vesicles is of interest both from a theoretical and experimental point of view, due to the fact that they serve as prototypical models for biological membranes.[1–10] Specifically, amphipathic phospholipids with hydrophilic headgroups and hydrophobic acyl tails tend to primarily form bilayers in aqueous solution in order to sequester their hydrophobic tails from unfavorable interactions with water. Cell membranes also contain macromolecules (e.g., proteins, carbohydrates) that enable a wide variety of functions, including transport across the membrane and cell-cell communication,[11] and have been implicated in the formation of complex membrane structures, such as the double membrane of autophagosomes.[12,13] In this work, we focus on the double lipid bilayer and propose one possible mechanism for the formation of this structure. Apart from the autophagosome, other eukaryotic cell organelles, including the nucleus, mitochondria, and chloroplasts are also surrounded by double membranes.[14] A physical understanding of the structure and dynamics of double lipid bilayers may thus aid our understanding of a wide range of biological phenomena.

Double-membrane organelles can either be long-lived or transient, and they are found across all branches of life.[15–18] Transient double-membrane organelles are formed under specific conditions and enable unique cellular processes, such as the forementioned autophagosomes that form during the self-digestion process (macroautophagy)[19,20]. The double membrane of the autophagosome serves an important function in the self-digestion process, as the outer membrane has to fuse with a lysosome containing digestive enzymes, which then degrade the inner lipid membrane of the autophagosome.[21] Apart from autophagosomes found in animal cells, plant cells contain chloroplasts with a characteristic double-membrane envelope, which has likely been developed from an engulfed cyanobacterial endosymbiont,[22] similar to the mitochondria in mammalian cells. In addition to organelles, all gram-negative bacteria have double-membrane envelopes, as well. These envelopes confer the bacteria with certain advantages, such as the ability to resist antibacterial agents and to adapt to a wide range of environmental conditions.[23] Although much is known about the machinery involved in the assembly of the membrane, the role of lipids and the basic physical mechanisms involved in the formation of such structures remain mysterious.[24] The evolutionary origin of such structures is also an active area of research.[25]

Here, we present a model of one possible physical mechanism for the spontaneous formation of double membrane vesi-

[a] Large Scale Structures Group, Neutron Scattering Division, Oak Ridge National Laboratory, Oak Ridge, TN 37831, United States
[b] Department of Physics and Astronomy, University of Tennessee, Knoxville, TN 37996, United States
[c] Shull-Wollan Center, Oak Ridge National Laboratory, Oak Ridge, Tennessee 37831, United States
[d] Center for Nanophase Materials Sciences, Oak Ridge National Laboratory, Oak Ridge, TN 37831, United States
[e] Computational Sciences and Engineering Division, Oak Ridge National Laboratory, Oak Ridge, TN 37831, United States
[*] E-mail: d.bolmatov@gmail.com
[‡] E-mail: carrillojy@ornl.gov
[§] E-mail: mlavrent@utk.edu

cles via an interaction with headgroup-anchored molecules. Our approach is not specific to any particular organelle or small molecule, but rather gives some evidence of how double membrane formation may proceed. We thereby supply some physical insight into one plausible avenue for the formation of this commonly-found, biologically-relevant structure. This work, which treats membrane dynamics at a coarse-grained scale (allowing us to probe the long time scales associated with lipid phase separation, for example), complements recent simulation results of entire, specific organelles at shorter time scales.[26,27]

Understanding how double membranes are formed has both practical applications[28–30] and fundamental implications, for example, in virus-induced double-walled vesicles.[17,31–35] Use of double-membrane vesicles for drug delivery[36] may allow for better release control of their cargo.[37] Importantly, membrane structure and dynamics can be changed in the presence of exogenous headgroup-anchored molecules, such as melatonin.[38,39] We will consider the effects that these small molecules, such as short-chain alcohols, vitamins, and hormones, have on single-layer vesicles. In addition, we assume that the small molecules have some degree of orientation and prefer to arrange head-to-tail when in large concentrations, mimicking melatonin's behavior.[40] It is also known that membranes deform in the presence of small molecules, which may or may not be a desirable feature. For instance, photostabilizing agents used in fluorescence measurements have been shown to modify the mechanical properties of lipid bilayers.[41]

A key feature of biological membranes is their ability to form lateral lipid heterogeneities.[42] In living cells, these heterogeneities are currently thought to be highly dynamic and nanoscopic, making them difficult to observe directly.[43,44] However, it is known that in model lipid membranes with compositions similar to the plasma membrane, the corresponding lipid mixtures phase separate and form macroscopic domains.[45] Also, recent work on reconstituted membranes of the endoplasmic reticulum shows that lipid domains may be implicated in contact sites with other organelles.[46] So, although the direct observation of lipid domains in living membranes and organelles, in particular, remains elusive,[47] we may expect heterogeneous lipid compositions in both the plasma membrane and in membranes of organelles, an aspect which we will explore in this study. In the fluid state, any phase separation is likely to be of the liquid-liquid type, where lipids partition into liquid-ordered and liquid-disordered regions. These liquid phases are typically rich with unsaturated (low-temperature melting) and saturated (high-temperature melting) lipids. Importantly, cholesterol is predominantly found within the liquid-ordered domains.[48,49] Here, we simulate heterogeneities in the membrane by considering models with specific lipid interactions that can be tuned to favor either the phase-separated or mixed phase.

We will develop a physical model which includes small molecule-lipid interactions, lipid heterogeneity, and liquid-liquid phase separation dynamics. The paper is organized as follows: In the next section, we describe our simulation methods. In Section 3, we show that double membrane formation at high small molecule concentrations occurs via the nucleation and growth of a double bilayer region. We also analyze the elasticity of the membrane at smaller concentrations of the small molecule and show that the membrane bending modulus decreases with increasing small molecule concentration. We argue that the transition to the double membrane has a first-order character and is mediated by enhanced membrane undulations. We conclude with some discussions of the implications of this proposed mechanism in Section 4.

2 Methods

We take a coarse-grained approach to simulate the lipid membrane using a simple three-bead model developed by Deserno and colleagues.[50,51] We consider three different lipid types (green A, red B, and yellow C), shown in Fig. 1. Since we model the solvent implicitly by introducing thermal fluctuations to the lipid molecules, we also mimic the amphiphilic nature of the lipids using the appropriate interaction potentials between the beads constituting each molecule. We do this by choosing purely repulsive head-head and head-tail interactions, and attractive tail-tail interactions. Each bead experiences thermal fluctuations through a Langevin thermostat[52] with the friction coefficient τ^{-1} implemented in LAMMPS.[53,54] In the simulations, and the following analysis, all units are reduced, where $\tau = \sigma\sqrt{(m/k_BT)}$, σ, $m = 1$, and k_BT are the standard Lennard-Jones time, distance, mass, and thermal energy, respectively.

All of the repulsive interactions are described by a modified Lennard-Jones (LJ) potential, called the Weeks-Chandler-Anderson (WCA) potential,[55] given by:

$$U_{\mathrm{WCA}}(r) = 4\varepsilon_w[(b/r)^{12} - (b/r)^6 + 1/4]\theta(r_c - r), \qquad (1)$$

where $\theta(x)$ is the step function, $\varepsilon_w = 1\ k_BT$ is the potential strength, and $r_c \equiv 2^{1/6}b$ is the cutoff distance, given in terms of the effective size b of the interaction regions. This distance is chosen to terminate the potential just before the attractive portion. We choose $b = 0.95\sigma$ for any headgroup interactions and $b = 1$ for tail-tail interactions. The tail-tail interactions have, in addition, an attractive potential component given by:

$$U_{\cos}(r) = \begin{cases} -\varepsilon_c, & r < r_c \\ -\varepsilon_c \cos^2[\pi(r - r_c)/2w_c], & r_c \le r \le r_c + w_c \\ 0, & r > r_c + w_c \end{cases}, \qquad (2)$$

where $\varepsilon_c = 1\ k_BT$ is the attractive well depth. It follows, then, that for $r > r_c$ the potential smoothly approaches zero over a distance of w_c. The distance w_c will depend on the lipid type and is shown in Fig. 1. The three lipid beads and the two small molecule beads are connected by finitely extensible nonlinear elastic (FENE) bonds described by:

$$U_{\mathrm{FENE}}(r) = -\frac{1}{2}k_{\mathrm{bond}}r_o^2 \ln\left[1 - \left(\frac{r}{r_o}\right)^2\right], \qquad (3)$$

with $k_{\mathrm{bond}} = 30\ k_BT/\sigma^2$ and $r_o = 1.5\ \sigma$. In the case of the lipids, a bending potential is also included to maintain the molecular shape:

$$U_{\mathrm{bend}}(\alpha) = k_{\mathrm{bend}}\,[1 + \cos(\alpha)]\,, \qquad (4)$$

where α is the angle between the two unit vectors defined by the orientation from the middle lipid bead to the other two lipid beads (see schematic in Fig. 1). The minimum of Eq. (4) is at $\alpha = \pi$, which favors a co-linear lipid bead configuration. A k_{bend} of $20\,k_BT$ is used, which results in an approximate lipid persistence length of $19\,\sigma$.[56]

In order to maintain membrane fluidity, the membrane attractive interactions in Eq. (2) have to be carefully chosen. Cooke *et al.* showed that $w_c = 1.3\,\sigma$ is at the boundary of the unstable phase, while $w_c = 1.7\,\sigma$ is at the boundary of the gel phase.[50] In this study, we constrain w_c in the range from $1.3\,\sigma$ to $1.7\,\sigma$ for fluid membrane systems. The specific values of w_c for lipid tail-tail interactions are given in Fig. 1. Simulations are run up to time $3\times10^5\,\tau$, a value which is well into the coarsening kinetics regime via patch coalescence for a liquid-liquid phase separating system.[50] To perform the data analysis, the final $2\times10^4\,\tau$ of the simulation runs is extracted with a sampling interval of $50\,\tau$, or 401 trajectory frames. The vesicle patch size remains relatively unchanged over these last frames.

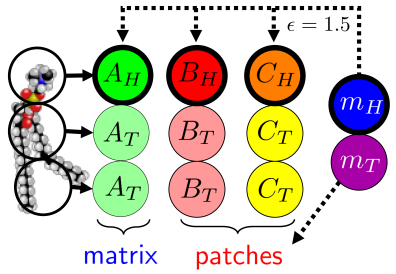

w_c , ϵ	A_T	B_T	C_T	m_T
A_T	1.5	1.5	1.3	0.5
B_T		1.5	1.7	1.5
C_T			1.3	1.5
m_T				0.5

Fig. 1 In the molecular dynamics simulations we consider four types of molecules, i.e., a ternary lipid mixture and a small molecule. Lipids are modeled using the coarse-grained approach by Cooke *et al.*.[50] A small molecule with a blue headgroup and a purple tail interacts with all the lipids with a truncated and shifted Lennard-Jones potential $U_{LJTS}(r)$ [Eq. (5)]. The head m_H prefers to bind to the lipid heads with the potential parameter $\epsilon = 1.5$ (in units of k_BT). The other values of ϵ for the m_T interactions with the other lipid tails are given in the table. We also list the cutoff values w_c of the tail-tail interactions given by Eq. (2) ($\epsilon_0 = 1\,k_BT$ here). All other interaction parameters are given in the main text.

The small molecules described here are designed to have short-range attractions between different types of lipid beads, thus mimicking different degrees of lipophilic interactions between the small molecule tail and lipid tails, and attractive interaction between the heads of small molecules and lipid heads, thereby biasing the small molecule's orientation towards the orientation of the lipid. That is, the tail-to-head direction of the small molecule is similar to the tail-to-head direction of neighboring lipids. This is similar to the orientations observed in small concentrations of lipid-associated small molecules and indoles, in particular. The interaction between small molecule beads to all other beads is described by a truncated and shifted Lennard-Jones potential,

$$U_{LJTS}(r) = 4\varepsilon\left[\left(\frac{b}{r}\right)^{12} - \left(\frac{b}{r}\right)^{6} - \left(\frac{b}{r_c}\right)^{12} + \left(\frac{b}{r_c}\right)^{6}\right]\theta(r_c - r), \tag{5}$$

with $r_c = 2.5\,b$ and $b = 0.95\,\sigma$, and the energy scale ε listed in Fig. 1. Note that these parameters introduce an attractive portion that mimics the hydrophobicity of the small molecule, which we expect to partition into the lipid bilayer, as opposed to the surrounding fluid.[57] In addition, small molecule hydrophobicity would favor aggregation.[58] To control this, we set the interaction between the head m_H and tail m_T with $\varepsilon = 2.0\,k_BT$ (and $b = 0.95\,\sigma$, $r_c = 2.5\,b$), which tends to favor small molecule aggregates with head-to-tail arrangements. Similar aggregates are conjectured for highly concentrated melatonin molecules near lipid headgroups.[40]

The initial spherical vesicle configuration consists of $N = 18996$ sites preassembled with an approximate radius of $30\,\sigma$ and an area per lipid of $1\,\sigma^2$ for both inner and outer leaflets.[59] The initial location of A lipids is in the matrix, B and C lipids in the patches, and the small molecules m are randomly distributed. The tested ranges of concentrations or number fractions for ϕ_A, ϕ_B, ϕ_C, and ϕ_m are $\{0.622-0.479\}$, $\{0.266-0.205\}$, 0.105, and $\{0.007-0.211\}$, respectively. This is done so that there is always a constant number of patches, which is determined by the interaction between the C and B lipids. The amounts of matrix lipids A and excess lipids B are adjusted with increasing amounts of the small molecules m, while maintaining a $\phi_A : \phi_B$ ratio of $0.7 : 0.3$. For comparison, we also consider homogeneous lipid membranes, where all the lipids are of the A type.

3 Results & Discussions

To explore the effect of small molecules on lipid phase separation and double-membrane formation, we consider four different lipid-small molecule interactions shown in Table 1. The two primary cases of interest are a single lipid type (Case 1) versus a three-component, phase-separating lipid mixture (Case 4), where the small molecule favors one of the lipid phases. As control systems, we consider the cases where the small molecule has no preference for the lipid phase (Case 2) and when m molecules prefer two of the lipid types, but where the lipids do not phase separate (Case 3). In addition to serving as a control on the effects of lipid phase separation, we expect the Case 3 to provide some insights into membranes of living cells, which tend to contain small transient domains, reminiscent of a disordered microemulsion phase.[60]

We also keep track of the critical concentration ϕ_m^* at which we observe the formation of a double membrane and compare the four cases. The cases where the small molecule partitions (Cases 3 and 4) have approximately *half* the critical value for ϕ_m^* compared to cases where the small molecule interacts the same way with all lipids (Cases 1 and 2). This advantage of partitioning is independent of lipid phase separation. The different critical concentration values ϕ_m^* for the different cases of lipid mixing and phase separation are shown in Table 1. Note that the value of ϕ_m^* is likely dependent on the simulation run, due to the first-

Case	Lipid	m molecule	ϕ_m^*
1	mixed	no preference	0.158
2	phase separated	no preference	0.145
3	mixed	prefers B/C	0.076
4	phase separated	prefers B/C	0.074

Table 1 The four different cases of lipid-small molecule m interactions. Case 1: single lipid type A; Case 2: all three lipid types with the small molecules interacting with the different lipids as if they were all type A; Case 3: the reverse of Case 2; and Case 4: all three lipid types and the small molecule m preferring the B/C lipid patches.

order-like behavior of the transition, something that we will discuss later on in the manuscript.

3.1 Small molecule partitioning

To begin, we need to test that our parameters for the small molecules m induce partitioning of m into the yellow/red lipid domains. This is shown in Fig. 2, where we calculate the density of m, where m has different interactions between B/C lipids versus A lipids (blue triangles) and compared to interactions as if all lipids are of type A (orange squares). These are, respectively, Cases 4 and 2, discussed previously (see Table 1). Recall that the attractive interactions between m and the lipids are given by Eq. (5), which has an attractive potential depth of ε. Furthermore, Fig. 1 shows that m has $\varepsilon = 1.5\ k_BT$ for the red/yellow B/C lipid tails versus $\varepsilon = 0.5\ k_BT$ for the green A lipids (in Case 3 and 4). Therefore, we expect that the relative density of m in the domains versus the patches can be approximated as: $\rho_m^{\text{domain}}/\rho_m^{\text{matrix}} \approx e \approx 2.7$. However, Fig. 2 shows that the ratio $\rho_m^{\text{domain}}/\rho_m^{\text{matrix}}$ is a bit larger than 3, implying additional preferential interactions such as a self-interaction of m due to the large $\varepsilon = 2.0\ k_BT$ responsible for the head-to-tail interaction. In addition, the ratio $\rho_m^{\text{domain}}/\rho_m^{\text{matrix}}$ remains relatively constant as a function of the m concentration ϕ_m.

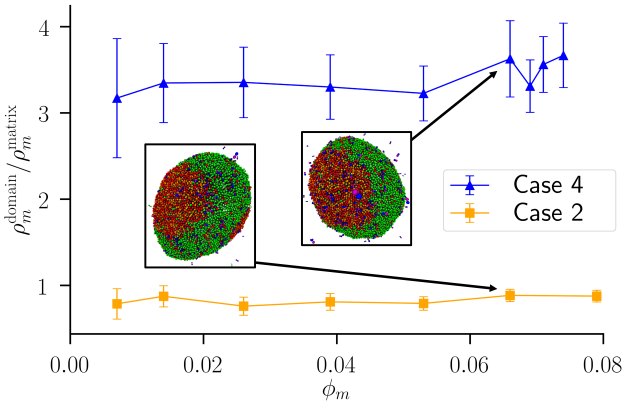

Fig. 2 We measured the areal density ratios of the small molecule m in the domains (red areas) and matrix (green areas) of lipid vesicles. In one case, we considered a vesicle, where m favors to partition into the domains (top line). In the other case (bottom line), m is insensitive to the lipid type. It is worth noting how different the densities are between the two cases. Additionally, we observe that not only does m prefer to partition into domains, it also facilitates the onion-like formation of vesicles.

One may also verify, qualitatively, that once the double membrane is formed, m preferentially resides between the two bilayers of the double-membrane vesicles, surrounded by lipid headgroups. This is clear for Case 1: Molecular dynamics simulation snapshots of double membrane formation (Fig. 3) show that as the double membrane forms, the molecules m (darker purple regions) partition into the middle of the double layer. The result is an overall decrease of m concentration on the outside of the vesicle, as can be verified by comparing the outer surfaces in panel i. and iv. of Fig. 3. The double membrane formation process is initiated by the nucleation and growth of a patch of double membrane, which we indicate with red arrows in Fig. 3.

A vesicle with a heterogeneous lipid composition also undergoes double membrane nucleation and the subsequent growth process, with an overall decrease of the m concentration on the outside of the vesicle. This process is shown in Fig. 4, where the initial double membrane patches are indicated with red arrows. We shall see later on that lipid composition heterogeneity promotes the formation of such structures (regardless of whether or not the lipids phase separate) as long as the small molecule prefers to bind to one of the lipid components. Note that the final double membrane vesicle in panel iv. has small molecules mostly sequestered between the two lipid bilayers.

Fig. 5 shows quantitative behavior of the small molecule m between bilayers in double-membrane vesicles for both uniform and heterogeneous lipid mixtures. Specifically, there is a sharp central peak in the density $\rho(\delta r)$ located near the midline of the vesicle double membrane, together with two smaller peaks near the outer leaflet headgroups. The dashed lines show the lipid headgroup densities, with the three peaks corresponding to the two outer leaflet headgroups and the layer between the two membranes where two sets of headgroups meet. We thus confirm that the majority of the small molecules reside between the two bilayers once the double layer vesicle has formed.

3.2 Elasticity considerations

In this section we focus on the elastic considerations in the transition from a single-membrane spherical vesicle to a double membrane. This, of course, is not the only possibility, and previous mechanical models of this type have focused on double membrane formation starting with a flat double-membrane sheet.[18] In our case, the double membrane forms only when there is a sufficient number of small molecules present. Moreover, fluctuations in the concentration of small molecules nucleate the beginnings of a double membrane. The process is shown for a homogeneous membrane (all green type-A lipids) in Fig. 3 using a series of simulation snapshots. Note the small piece of double membrane in panel iii. of Fig. 3. Due to the strong $m_H - A_H$ interactions (see Fig. 1), the small molecules prefer to sequester between the membranes where there is a high density of lipid headgroups.

The energetically favorable location of the small molecules between the two membranes is compensated by an increase in bending energy for double-membrane lipid vesicles. A single-membrane lipid vesicle resists bending, and the bending energy associated with forming a spherical vesicle is given by the integral

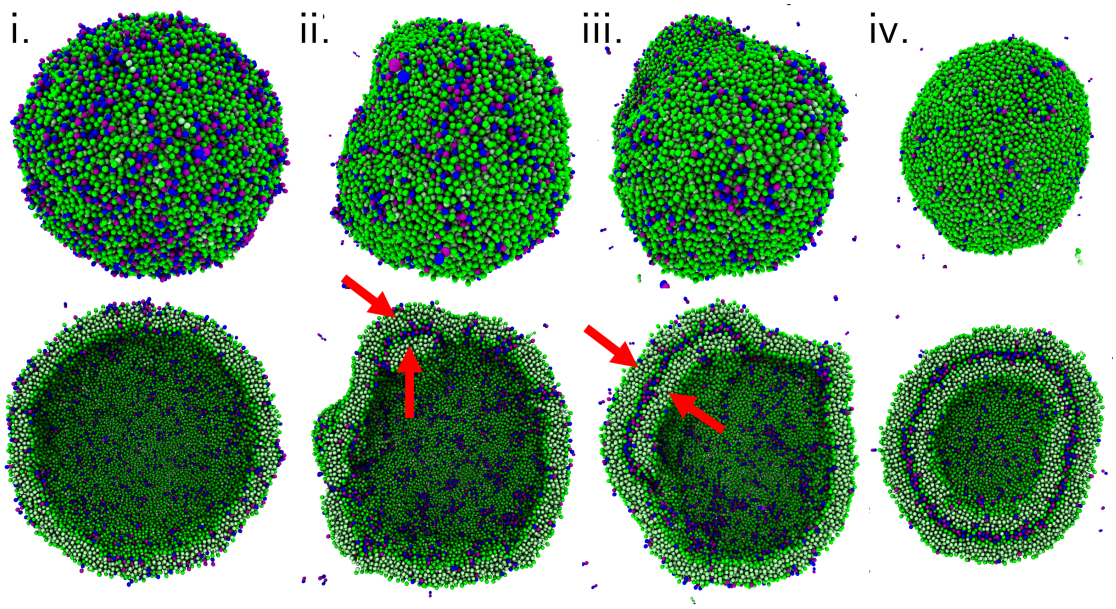

Fig. 3 Double-membrane formation in a green, homogeneous lipid vesicle in the presence of a small molecule m (blue/purple), that favors to reside near the lipid headgroups (Case 1 in Table 1), which are all of type A (see Fig. 1). The m fraction is $\phi_m = 0.198$. Various molecular dynamics snapshots are shown (going left to right from i. to iv.): 0, 10^6, 1.2×10^6, and 5×10^6 time steps. The panels on top show the outer surface, while those in the bottom are cross sections through the vesicle. At intermediate times (panels ii. and iii.), we find various stages of formation during which the small molecule m clusters into small domains and eventually nucleates a double membrane which spreads and forms the full double-membrane vesicle. The red arrows indicate the nucleation and propagation of a patch of two bilayers "glued" together by the purple small molecules.

of the energy over the membrane surface A, written as follows:

$$E_b = \int \mathrm{d}A\, \frac{\kappa}{2}(c_1+c_2)^2 = 8\pi\kappa, \tag{6}$$

where $c_{1,2} = 1/R$ are the principal curvatures of a spherical surface with radius R, and where κ denotes the bending modulus. The bending modulus can be explicitly evaluated by flicker spectroscopy[50,59] and neutron spin echo spectroscopy.[61] Importantly, the bending energy is independent of the vesicle radius R. One may also include a Gaussian curvature term proportional to the Gaussian curvature modulus $\bar{\kappa}$. This term is only relevant when the membrane topology changes, which would be at large ϕ_m near the phase transition between the single- and double-membrane vesicle. Also, the modulus $\bar{\kappa}$ requires special techniques to measure.[62]

The bending rigidity κ depends on the concentration ϕ_m of the small molecule and is different for a single-membrane versus a double-membrane vesicle. In a double-membrane vesicle, if the two membranes were completely decoupled, we would naturally have $\kappa_2 = 2\kappa$. However, since the small molecules reside in the interstitial region, the two membranes are not free to slide one relative to the other. In this case, we would expect the bending rigidity to be larger due to the suppression of shear. For a membrane made of a homogeneous elastic material, we know that $\kappa \propto h^3$, where h is the membrane thickness. Lipid membranes, however, are known to have bending rigidity parameters that scale like $\kappa \propto h^2$.[63] Hence, we can expect that double membranes have some range of bending rigidities, i.e., $\kappa_2 = (2-8)\kappa$. Therefore, the double membrane configuration requires some mitigation of the bending energy via the sequestering of the small molecules between the lipid bilayers.

A proper estimate of the double-membrane vesicle elasticity is beyond the reach of our simple analysis, due to the large rearrangements of the membrane that occur during the double bilayer formation (see Fig. 3 and Fig. 4). Our elastic model is limited to nearly-spherical membrane shapes and the transition region likely involves topological changes. An elastic model of the transition region would require an estimate of the Gaussian bending modulus $\bar{\kappa}$. Instead, we will now analyze the elasticity of the spherical vesicle away from the transition, at small concentrations $\phi_m < \phi_m^*$. Here, we expect to find an approximately spherical vesicle for which we can perform flicker spectroscopy analysis. We shall see in the following that, surprisingly, the vesicle maintains a spherical shape all the way up to the transition point, i.e. $\phi_m \approx \phi_m^*$, rendering our flicker spectroscopy analysis valid over a wider range of concentrations than anticipated.

We check the membrane elasticity considerations by measuring the effective bending rigidity κ for small concentrations ϕ_m (i.e., before the double-membrane transition). In this case, the vesicle has one bilayer and is thin enough that one may determine κ via flicker spectroscopy. In particular, we may analyze the midline $\mathbf{R}(\theta,\phi)$ of the membrane. To begin with, we assume that membrane undulations are small and do not modify the vesicle topology. Therefore, we can expand $\mathbf{R}(\theta,\phi) = R_V[1+\sum_{\ell,m} u_\ell^m Y_\ell^m(\theta,\phi)]\hat{\mathbf{r}}$, where R_V is the radius of a sphere that yields the vesicle volume $V = 4\pi R_V^3/3$ and $Y_\ell^m(\theta,\phi)$ are spherical harmonics. The modes u_ℓ^m for $\ell = 0,1,2,\ldots$ and $m = -\ell,-\ell+1,\ldots,\ell$ describe the membrane undulations which perturb the vesicle from its spherical shape. Substituting this parameterized shape into the Helfrich free energy of the kind in Eq. (6), along with a surface tension term ΣA

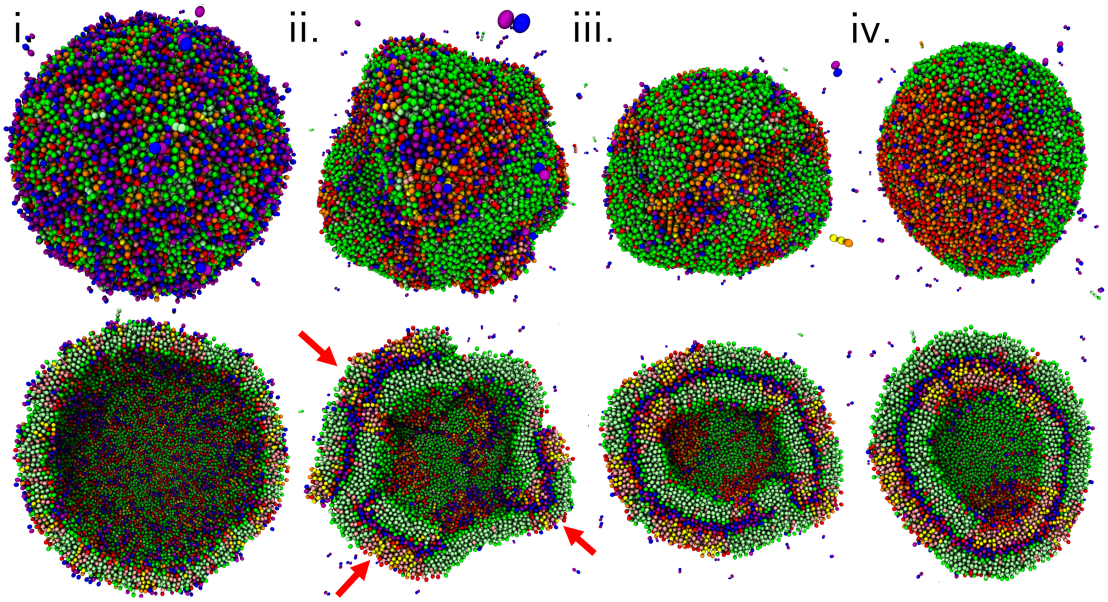

Fig. 4 Double-membrane formation in a phase-separating vesicle in the presence of a small molecule m (blue/purple), that favors partitioning into the red/yellow patches of lipids (Case 4 in Table 1). The m fraction is $\phi_m = 0.211$. Molecular dynamics simulation snapshots (from left to right) for: 0, 0.4×10^6, 0.6×10^6, and 10^7 time steps. The panels on top show the outer surface, while the bottom ones are cross sections through the vesicle. At intermediate times, we find various stages of double-membrane formation during which the small molecule m "sticks" two bilayers at different locations of the double-membrane. These places are indicated by the red arrows in the bottom panel of ii. Note that the vesicle becomes highly irregular at step ii., consistent with our observation of reduced membrane rigidity with increasing ϕ_m.

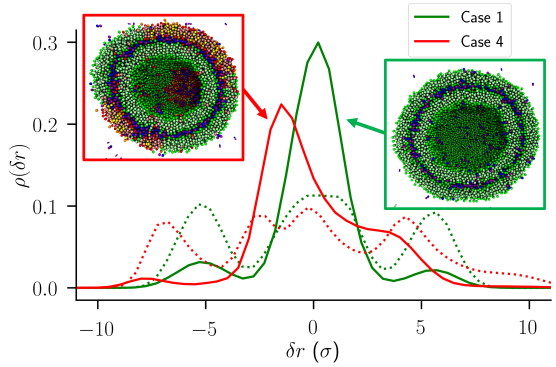

Fig. 5 The relative density ρ of small molecule headgroups m_H (solid lines) and lipid headgroups (dashed lines) as a function of distance δr from the midline of the double membrane. ρ for both molecules is normalized so that $\int \mathrm{d}r\,\rho(r) = 1$. The large solid line peaks near $\delta r = 0$ show that most of the small molecules reside between the two bilayers as these solid line peaks coincide with the central dashed line peaks which correspond to the lipid headgroups located between the two bilayers of the double membrane.

that penalizes membrane stretching, yields a total (free) energy for the modes u_ℓ^m, which can be written[64] as follows:

$$\mathscr{E} = \text{const} + \frac{\kappa}{2}\sum_{\ell,m} |u_\ell^m|^2(\ell+2)(\ell-1)[\ell(\ell+1)+\bar{\sigma}], \qquad (7)$$

with $\bar{\sigma} = \bar{\Sigma}R_V^2/\kappa$. The energy $\mathscr{E}$ can now be used as a Boltzmann weight to estimate the magnitude of fluctuations of a particular mode u_ℓ^m.[65] By monitoring the fluctuations and taking an average $\langle|u_\ell^m|^2\rangle$, we can fit the mode averages to the bending rigidity κ and the re-scaled surface tension $\bar{\sigma}$. Specifically:

$$\langle|u_\ell^m|^2\rangle = \frac{k_BT}{\kappa}\,[(\ell+2)(\ell-1)[\ell(\ell+1)+\bar{\sigma}]^{-1}\,. \qquad (8)$$

Fig. 6 shows a plot of the bending rigidity κ decreasing monotonically with ϕ_m. First, we note that at very small ϕ_m, our results are consistent with previous work[50,59] showing that the bending modulus of the model membrane is $\sim 10k_BT$ - for our choice of parameters. As we increase ϕ_m, the bending rigidity κ decreases. Indeed, near the critical concentrations ϕ_m^* (see Table 1), and particularly for Case 1 and 2, the bending rigidity is significantly smaller than the membrane without any small molecules. In Case 3 and 4, the decrease is not as dramatic. Two reasons for this are: (i) We measure κ over a much smaller range of ϕ_m as the phase transition (where our approximation breaks down) occurs at smaller ϕ_m for Cases 3 and 4; and (ii) In these cases, the small molecule preferentially binds to the B/C lipids and it is likely that κ is not homogeneous throughout the membrane due to increased clustering of the small molecules. We see evidence of this in the larger error bars for κ at higher ϕ_m for these cases (bottom panel of Fig. 6). We will explore this aspect later when we discuss the distribution and orientation of the small molecules. Nevertheless, in all cases, our results point to a decrease in effective κ, implying large fluctuations as being an explicit feature of a transition in vesicle topology. This behavior is consistent with the transitions shown in Figs. 3 and 4. The membrane locally undulates and rearranges to nucleate a double membrane.

A limitation of our flicker spectroscopy analysis is that we assume the vesicle shape does not deviate to any great extent from a sphere. We have verified that for all the concentrations ϕ_m shown

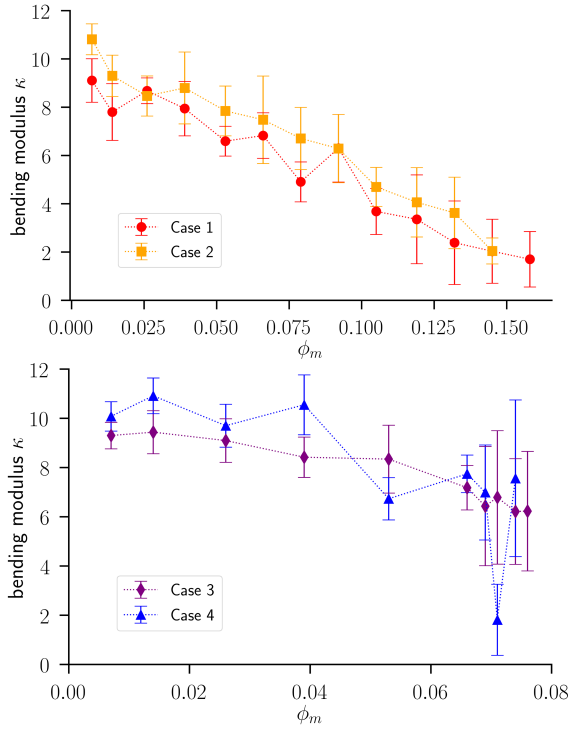

Fig. 6 The bending rigidity κ (in units of k_BT) for the four different cases tabulated in Table 1, plotted as a function of the small molecule concentration ϕ_m. The data are presented up to the critical value ϕ_m^*, when the double-membrane transition occurs. The values of κ are calculated by averaging the mode fluctuations over different time frames of the simulations [see Eq. (8)]. The error bars are standard deviations calculated based on a bootstrapping method. Note how κ decreases with ϕ_m, facilitating the membrane undulations responsible for generating the double membrane.

in Fig. 6, the average radial position of the molecules does not deviate from R_V by more than 15%. Indeed, the vesicle remains roughly spherical all the way up to the double layer transition for a sufficiently large ϕ_m. The smaller bending rigidity indicates a propensity for larger undulations away from the spherical shape as ϕ_m increases, but the spherical geometry is maintained for $\phi_m < \phi_m^*$. This is an indication that the spherical shape remains stable up to the double membrane transition and is likely metastable near the transition region, which is a signature of a first-order transition. One may also speculate on the temperature dependence of our results. For our particular lipid model, changing the value of w_c can tune κ between k_BT at high temperatures and $30k_BT$ at lower temperatures (within the range of parameters where the membrane maintains fluidity).[50,59] Thus, we may expect that double membrane formation occurs more readily at higher temperatures, where the bending modulus is smaller. In the future, it would be interesting to run a temperature scan to examine this effect in more detail.

Topological changes in fluid membranes are known to be controlled both by the bending rigidity κ and pressure difference between the inside and outside of the vesicle.[66] First-order transitions between vesicle and branched polymer-like phases, and between open and closed topologies, are common and generally expected to be first-order.[67] The single to double-membrane transition is an example of such a transition, and our measurement of κ suggests that it is precisely the decrease in the effective κ that drives the transition. It would be interesting to also measure the pressure change across the vesicle. However, the use of an implicit solvent precludes a precise measurement of this quantity.

3.3 Metastable states and dynamics near ϕ_m^*

It is intriguing to consider vesicles at large values of ϕ_m and near the transition $\phi_m \approx \phi_m^*$ (see Table 1). Recall that at increasing concentrations of m, we find reduced bending rigidities κ and greater probability to come across undulated and highly deformed vesicles. Due to the large deformations, the value of κ is difficult to measure at the transition $\phi_m \approx \phi_m^*$. So, instead of calculating κ, we simulated multiple vesicles at large values of ϕ_m, with final results shown in Fig. 7. The morphologies that we find at large $\phi_m > \phi_m^*$ are not necessarily perfectly-shaped double membranes, but include some interesting "intermediate" morphologies shown in Fig. 7. These morphologies are apparently metastable (persisting up to the longest simulation times) and occur in both uniform [Fig. 7(a)] and phase-separating lipid mixtures [Fig. 7(b)], and appear to be some combination of single and double-membrane morphologies, including lamellar structures with lipid bilayers alternating with high concentrations of m [see center and right panels of Fig. 7(a), for example].

The various transition states in Fig. 7 suggest that there are local free energy minima associated with the double-membrane transition, which is likely hysteretic and a first-order transition. Fig. 7 indicates that we may find very different intermediate states given just small variations in ϕ_m, meaning that the double-membrane free energy landscape is populated with many local minima. We also find coexistence between single-membrane and double-membrane structures, as seen in the left panel of Fig. 7(a) and in the structures in Fig. 7(b). This is indicative of a first-order transition between the two kinds of membrane structures. Note that the presence of the small molecules can generate areas of high curvature, as shown by the red arrow in the left panel of Fig. 7(b). Here, the particles may serve as curvature-generating inclusions for the lipid membrane. It may thus be possible to understand some of these intermediate states in an elastic model by incorporating a coupling between the small molecule concentration and the membrane curvature.[68]

We may now consider the dynamics of vesicles at these high ϕ_m values. Fig. 8(a) shows the pair-wise interaction energies for simulation runs near and above the critical ϕ_m^* as a function of time. The transition to a double membrane is marked by a rapid, spontaneous decrease in the interaction energies, and sharp drops indicate where the double membrane forms – no signature of the first-order transition is observed prior to any drop. This suggests that the process of double membrane formation is driven by membrane fluctuations rather than some deterministic flow of the simulation trajectory from a single- to double-membrane morphology. The transition takes place when the membrane fluctuations nucleate a patch of double membrane that eventually propagates across the entire membrane. We can compare, for example, the

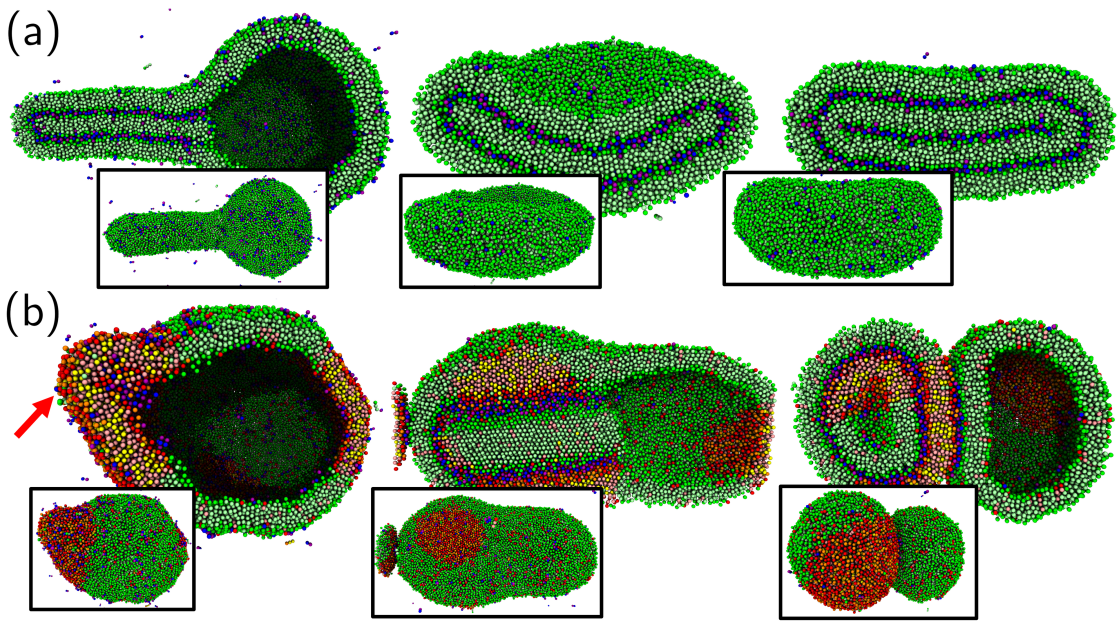

Fig. 7 Different morphologies of uniform (a), at small molecule concentrations $\phi_m = 0.164, 0.166, 0.185$ going from left to right and of phase separated vesicles (b) for concentrations $\phi_m = 0.076, 0.079, 0.092$ from left to right. Small variations in the small molecule fraction ϕ_m can lead to substantial changes in simulation results, suggesting that the energy landscape for these systems has many local minima, which include combinations of double-membranes and single bilayer vesicles. The simulation periodic boundary conditions also allow for lamellar structures to form. A partial lamella is observed for $\phi_m = 0.079$ [middle panel of (b)]. Note that in the case of (b), small molecules prefer to aggregate in the red/yellow patches, which are also more likely to nucleate the double-membrane structure. All figures are snapshots from simulations with at least 10^7 time steps. The red arrow in the left panel of (b) indicates a place where the small molecules induce a sharp change in the membrane curvature.

pair energies in Case 4 shown for $\phi_m = 0.074$ and $\phi_m = 0.079$ in Fig. 8(a). Note how the curve for the latter concentration drops down sharply at around $\tau \approx 2.5 \times 10^5$. This corresponds to the formation of a multilamellar patch, which nucleates and then grows. The middle panel of Fig. 7(b) shows the final state of the $\phi_m = 0.079$ case, where we see that the system gets stuck in an intermediate state with both a single- and double-membrane portion.

In Fig. 8(b) we show the pair-wise interaction energy for the same simulation shown in Fig. 3. The vertical dashed lines indicate the times at which we take the simulation snapshots in panel ii. and iii. in Fig. 3. Note that as soon as the double membrane nucleates (panel ii. in Fig. 3), the pair-wise energy drops and eventually approaches a new constant, corresponding to the double membrane vesicle. The transition happens relatively rapidly, and there is no clear indication when precisely the double membrane patch will first nucleate. This is indicative of a first-order transition behavior, where the single-layered structure becomes metastable at the transition and requires fluctuations to overcome the free energy barrier to the formation of a local double membrane patch.

3.4 Molecule orientation and concentration

It is also interesting to look into the density and orientation of the small molecules and lipids during the single- to double-membrane transition. We monitor the density of lipids and small molecules m for small and large values of ϕ_m in Fig. 9 for homogeneous, single-membrane lipid vesicles. We notice that at low ϕ_m, the small molecule density is registered with the lipid headgroups across the two membrane leaflets: i.e., see the two peaks in the blue curves shown in Fig. 9 where the dashed and solid lines have the same shape. This makes sense as the small molecule does not differentiate between lipids, but simply favors to remain near the lipid headgroups. At increased ϕ_m (red curves), the densities become asymmetric, which is a signature of local bending of the bilayer. We also see that the bilayer dilates (on average), likely corresponding to the formation of locally-deformed, double-membrane regions. Similar density profiles can be found for the cases with heterogeneous lipid mixtures (i.e., Case 2-4), although the various lipid types and the small molecules have a non-uniform distribution in these cases, making a spherical average (as was done in Fig. 9) difficult to interpret.

At high concentrations of ϕ_m, we also expect that the small molecules will reorient and align perpendicular to the membrane. This orientation then facilitates the preferential head-to-tail arrangement of the small molecules in our simulations. One way to track small molecule orientation is to measure the P_2 order parameter, given by:

$$P_2 = \frac{1}{2}\left[3\left\langle(\hat{\mathbf{m}}\cdot\hat{\mathbf{r}})^2\right\rangle - 1\right], \tag{9}$$

where $\hat{\mathbf{r}}$ is the radial direction (the normal, on average, to the spherical vesicle membrane) and we average over all orientations (head-to-tail directions) $\hat{\mathbf{m}}$ of the small molecules. We see that the parameter ranges from $P_2 = -1/2$ for when molecules are perpendicularly oriented $\hat{\mathbf{r}} \perp \hat{\mathbf{m}}$ and $P_2 = 1$ for parallel orientation $\hat{\mathbf{r}} \parallel \hat{\mathbf{m}}$

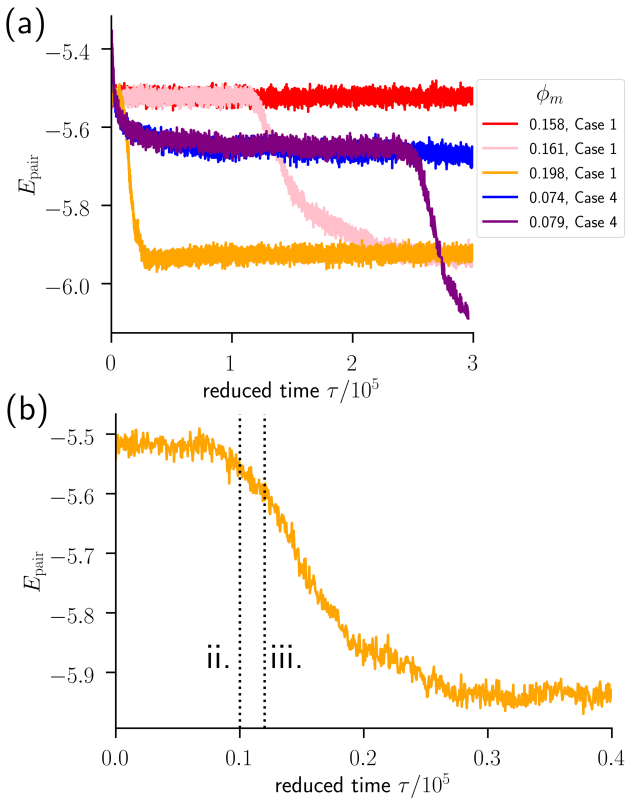

Fig. 8 (a) We show the pair-wise interaction energy between atoms obtained from molecular dynamics simulations as a function of reduced time τ, which is the integration time step (0.01) multiplied by the number of simulation time steps. Simulation runs with small molecule fractions ϕ_m around the critical density ϕ_m^* are shown. For Case 4 plots, the different states at the longest simulation times are shown in Fig. 7. (b) Zoomed in trace of the pair-wise interaction energy for the Case 1 vesicle with $\phi_m = 0.198$, for which we showed snapshots in Fig. 3. The vertical dashed lines indicate the times of the corresponding snapshots in Fig. 3. As soon as the double membrane nucleates and spreads across the surface, the free energy decreases to a new minimum corresponding to a double membrane vesicle.

– a random orientation would yield $P_2 = 0$. We observe in Fig. 10 that as we increase ϕ_m, the small molecules tend to reorient in a direction that, on average, is less parallel to the lipid direction. A dramatic difference is seen when the small molecules partition preferentially into one of the lipids [see the blue and purple (Case 3,4) lines in Fig. 10 versus the red and orange ones (Case 1,2)]. This is likely due to the fact that the molecules m are locally highly concentrated in Case 3 and 4 and should be more likely to self-interact and form head-to-tail aggregates. Also, this reorientation most likely favors double membrane formation, a notion that is borne out in the differences in critical concentrations ϕ_m^* between the partitioning and non-partitioning cases (see Table 1). In the double-membrane configuration, the small molecule orientations are close to random, as can be seen by the points to the right of the vertical lines in Fig. 10, which indicate the critical ϕ_m^*.

Biomolecule reorientation is commonly observed in many small lipid-associated molecules, including melatonin, cholesterol, and steroids.[69] The nature of the reorientation transition, though, is sensitive to the lipid and small molecule types.[70,71] The small

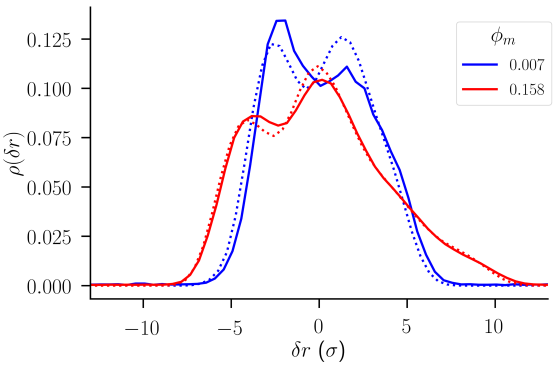

Fig. 9 The relative density ρ of small molecule headgroups m_H (solid lines) and lipid headgroups A_H (dashed lines) as a function of distance δr from the center of mass of the lipid bilayer, averaged over the entire (single membrane) vesicle and over the last 401 frames of our molecular dynamics simulation for Case 1 (see Table 1). ρ was normalized such that $\int \mathrm{d}r\, \rho(r) = 1$. Small (blue) and large (red) concentrations ϕ_m near ϕ_m^* of the small molecule are shown. As ϕ_m increases, the distribution widens and the molecule/lipid distribution becomes more asymmetric due to the enhanced undulations that facilitate double-membrane formation.

molecules in our simulations mimic melatonin's behavior, which has been shown to reorient from a parallel to a perpendicular orientation, with respect to the lipid molecules in the bilayer, with increasing concentration.[40] However, we note that our model is purely phenomenological and does not correspond to a specific small molecule. Finally, these results also indicate that a relatively simple interaction can lead to morphological transformations and complex behavior, including a collective reorientation of small biomolecules accompanying the single- to double-membrane vesicle transition.

4 Conclusions

We examined, in detail, the formation of double-membrane vesicles from single-membrane vesicles in the presence of small hydrophobic biomolecules. We showed that small molecules induce a first-order-like phase transition, where the double-membrane morphology nucleates and then propagates over the entire vesicle surface. Small molecules facilitate these processes by decreasing the effective bending rigidity of the membrane, thus increasing the probability for large scale membrane fluctuations and membrane reorganization to take place. One interesting possibility is that local concentration fluctuations of the small molecules serve as curvature-inducing inclusions for the lipid membrane. One might be able to verify this by comparing our molecular-scale model to a fully elastic model, where the small molecule-membrane interactions would be treated as coupling terms in a Helfrich free energy of the kind described by Eq. (4).[68] The properties of the initial nucleus of the double membrane would be interesting to explore, as well. We would expect a free energy barrier to the formation of this nucleus, which could be explored focusing on the small patch of the vesicle that first forms the double layer.

We have also examined the effects of a heterogeneous lipid composition on the double layer formation. We found that as long as the small molecules prefer to bind to one of the lipid

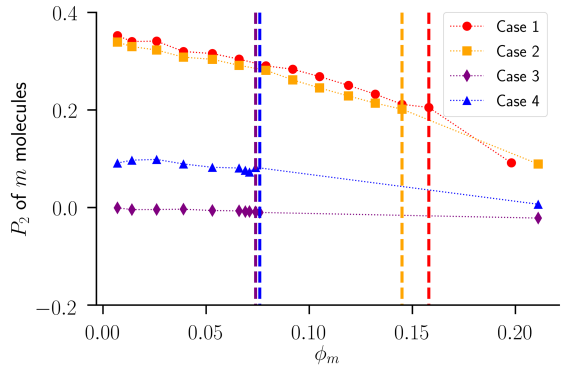

Fig. 10 Orientation parameter P_2 of the small molecule m as a function of small molecule fraction ϕ_m of m in the vesicle's composition. Increasing the amount of m tends to force the small molecules to transition from an orientation that is parallel to the lipids ($P_2 \sim 1$) to one that is more random or perpendicular ($P_2 < 0$). The vertical lines show the critical concentration ϕ_m^* beyond which we find double-membranes for the different interaction parameters (see Table 1). The single points to the right of each vertical line are the orientations of the small molecules in a double-membrane vesicle corresponding to the given case.

components, the double layer formation is enhanced (the critical value of ϕ_m^* decreases by about a factor of 2), whether or not the lipids phase separate. Thus, we may expect that such small molecules would also enhance double membrane formation in living membranes where the lipid composition is heterogeneous but not necessarily phase separated into large domains.

We found that double-membrane formation is accompanied by small molecule reorientation and aggregation between lipid bilayers. We expect to find such behavior in a wide range of systems where small hydrophobic molecules interact with lipid headgroups. In this regard, it is intriguing to compare the obtained results from our coarse-grained simulations to those of all-atom simulations.[71] Current simulation techniques are able to capture entire organelles with atomic resolution, albeit at limited time scales.[27] It would be interesting to compare our work with these more detailed simulations. The advantage of our approach is that we are able to simulate the small molecule-lipid interactions over much larger time and length scales, thus capturing the collective membrane undulations. In the future, it would be possible to use atomistic simulations to inform the interaction parameters for our coarse-grained model. In addition, it may be possible to couple multiple time- and length-scales using recently developed multiscale simulation approaches.[26]

Conflicts of interest

There are no conflicts to declare.

Acknowledgements

This research was performed at the Center for Nanophase Materials Sciences, which is a US Department of Energy Office of Science User Facility. This research used resources of the Oak Ridge Leadership Computing Facility at the Oak Ridge National Laboratory, which is supported by the Office of Science of the U.S. Department of Energy under Contract No. DE-AC05-00OR22725. M. O. L. was supported by the Neutron Sciences Directorate (Oak Ridge National Laboratory), sponsored by the Department of Energy, Office of Basic Energy Sciences. J.K. is supported through the Scientific User Facilities Division of the Department of Energy (DOE) Office of Science, sponsored by the Basic Energy Sciences (BES) Program, under Contract No. DE-AC05-00OR22725.

References

1 W. Helfrich, *Z. Naturforsch C.*, 1973, **28**, 693–703.
2 M. F. Eckenhoff and J. J. Pysh, *J. Neurocytol.*, 1979, **8**, 623–638.
3 U. Seifert, K. Berndl and R. Lipowsky, *Phys. Rev. A*, 1991, **44**, 1182.
4 K. W. Pedersen, Y. van der Meer, N. Roos and E. J. Snijder, *J. Virol.*, 1999, **73**, 2016–2026.
5 P. Paradisi, P. Allegrini and D. Chiarugi, *BMC Syst. Biol.*, 2015, **9**, S7.
6 D. Bolmatov, Y. Q. Cai, D. Zav'yalov and M. Zhernenkov, *Biochim. Biophys. Acta Biomembr.*, 2018, **1860**, 2446–2455.
7 A. H. Bahrami, M. G. Lin, X. Ren, J. H. Hurley and G. Hummer, *PLOS Comput. Biol.*, 2017, **13**, e1005817.
8 F. Campelo, J. van Galen, G. Turacchio, S. Parashuraman, M. M. Kozlov, M. F. Garcia-Parajo and V. Malhotra, *Elife*, 2017, **6**, e24603.
9 V. N. Anghel, D. Bolmatov and J. Katsaras, *Phys. Rev. E*, 2018, **97**, 062405.
10 D. Bolmatov, D. Zav'yalov, J.-M. Carrillo and J. Katsaras, *Biochim. Biophys. Acta Biomembr.*, 2020, 183249.
11 Z. Cournia, T. W. Allen, I. Andricioaei, B. Antonny, D. Baum, G. Brannigan, N.-V. Buchete, J. T. Deckman, L. Delemotte, C. del Val, R. Friedman, P. Gkeka, H.-C. Hege, J. Hénin, M. A. Kasimova, A. Kolocouris, M. L. Klein, S. K. M. J. Lemieux, N. Lindow, M. Roy, J. Selent, M. Tarek, F. Tofoleanu, S. Vanni, S. Urban, D. J. Wales, J. C. Smith and A.-N. Bondar, *J. Membrane Biol.*, 2015, **248**, 611–640.
12 W.-L. Yen, T. Shintani, U. Nair, Y. Cao, B. C. Richardson, Z. Li, F. M. Hughson, M. Baba and D. J. Klionsky, *J. Cell Biol.*, 2010, **188**, 101–114.
13 N. Mizushima, T. Yoshimori and Y. Ohsumi, *Annu. Rev. Cell Dev. Biol.*, 2011, **27**, 107–132.
14 Y. Yoshida, Y. Sakamoto, K. Iwasaki, S. Maruyama and S. Matsunaga, in *Cyanidioschyzon merolae*, Springer, 2017, pp. 205–233.
15 S. Miller and J. Krijnse-Locker, *Nat. Rev. Microbiol.*, 2008, **6**, 363–374.
16 D. H. Murray, L. K. Tamm and V. Kiessling, *J. Struct. Biol.*, 2009, **168**, 183–189.
17 C. L. Netherton and T. Wileman, *Curr. Opin. Virol.*, 2011, **1**, 381–387.
18 R. L. Knorr, R. Dimova and R. Lipowsky, *PLoS One*, 2012, **7**, e32753.
19 N. Mizushima, *Nat. Cell Biol.*, 2018, **20**, 521.
20 N. Mizushima, B. Levine, A. M. Cuervo and D. J. Klionsky, *Nature*, 2008, **451**, 1069–1075.
21 M. Hamasaki, S. T. Shibutani and T. Yoshimori, *Curr. Opin.*

Cell Biol., 2013, **25**, 455–460.
22 K. Inoue, *Trends Plant Sci.*, 2011, **16**, 550–557.
23 J. W. Costerton, J. M. Ingram and K.-J. Cheng, *Microbiol. Rev.*, 1974, **38**, 87–110.
24 M. P. Bos and J. Tofmmassen, *Curr. Opin. Microbiol.*, 2004, **7**, 610–616.
25 D. Megrian, N. Taib, J. Witwinowski, C. Beloin and S. Gribaldo, *Mol. Microbiol.*, 2020, **113**, 659–671.
26 W. Pezeshkian, M. König, T. A. Wassenaar and S. J. Marrink, *Nat. Commun.*, 2020, **11**, 2296.
27 A. Singharoy, C. Maffeo, K. H. Delgado-Magnero, D. J. Swainsbury, M. Sener, U. Kleinekathöfer, J. W. Vant, J. Nguyen, A. Hitchcock, B. Isralewitz, I. Teo, D. E. Chandler, J. E. Stone, J. C. Phillips, T. V. Pogorelov, M. I. Mallus, C. Chipot, Z. Luthey-Schulten, D. P. Tieleman, C. N. Hunter, E. Tajkhorshid, A. Aksimentiev and K. Schulten, *Cell*, 2019, **179**, 1098–1111.e23.
28 Y.-C. Li, Y.-N. Li, C.-X. Cheng, H. Sakamoto, T. Kawate, O. Shimada and S. Atsumi, *Neurosci. Res.*, 2005, **53**, 298–303.
29 A. S. Wang, A. Kundu, B. Fong, J. Fitzgerald, B. Larijani and D. Poccia, *Biol. Bull.*, 2013, **224**, 218–226.
30 G. Wolff, C. E. Melia, E. J. Snijder and M. Bárcena, *Trends Microbiol.*, 2020, 1.
31 R. Gosert, A. Kanjanahaluethai, D. Egger, K. Bienz and S. C. Baker, *J. Virol.*, 2002, **76**, 3697–3708.
32 A. Moshe and R. Gorovits, *Viruses*, 2012, **4**, 2218–2232.
33 M. M. Angelini, M. Akhlaghpour, B. W. Neuman and M. J. Buchmeier, *mBio*, 2013, **4**, e00524–13.
34 A. Lundin, R. Dijkman, T. Bergström, N. Kann, B. Adamiak, C. Hannoun, E. Kindler, H. R. Jonsdottir, D. Muth, J. Kint, M. Forlenza, M. A. Muller, C. Drosten, V. Thiel and E. Trybala, *PLoS Pathog.*, 2014, **10**, e1004166.
35 G. Ávila-Pérez, M. T. Rejas and D. Rodríguez, *Cell. Microbiol.*, 2016, **18**, 1691–1708.
36 T. M. Allen and P. R. Cullis, *Adv. Drug Deliv. Rev.*, 2013, **65**, 36–48.
37 P. Sahu, S. K. Kashaw, S. Jain, S. Sau and A. K. Iyer, *J. Control. Release*, 2017, **253**, 122–136.
38 D. Bolmatov, W. T. McClintic, G. Taylor, C. B. Stanley, C. Do, C. P. Collier, Z. Leonenko, M. O. Lavrentovich and J. Katsaras, *Langmuir*, 2019, **35**, 12236–12245.
39 D. Bolmatov, D. Soloviov, M. Zhernenkov, D. Zav'yalov, E. Mamontov, A. Suvorov, Y. Q. Cai and J. Katsaras, *Langmuir*, 2020, **36**, 4887–4896.
40 H. Dies, B. Cheung, J. Tang and M. C. Rheinstädter, *Biochim. Biophys. Acta*, 2015, **1848**, 1032–1040.
41 J. L. Alejo, S. C. Blanchard and O. S. Andersen, *Biophys. J.*, 2013, **104**, 2410–2418.
42 M. Sahebifard, A. Shahidi and S. Ziaei-Rad, *Eur. Biophys. J.*, 2017, **46**, 343–350.
43 J. D. Nickels, S. Chatterjee, C. B. Stanley, S. Qian, X. Cheng, D. A. Myles, R. F. Standaert, J. G. Elkins and J. Katsaras, *PLOS Biol.*, 2017, **15**, e2002214.
44 E. Sezgin, I. Levental, S. Mayor and C. Eggeling, *Nat. Rev. Mol. Cell Biol.*, 2017, **18**, 361.
45 S. L. Veatch and S. L. Keller, *Biophys. J.*, 2003, **85**, 3074–3083.
46 C. King, P. Sengupta, A. Y. Seo and J. Lippincott-Schwartz, *Proc. Natl. Acad. Sci. U.S.A.*, 2020, **117**, 7225–7235.
47 G. v. Meer, D. R. Voelker and G. W. Feigenson, *Nat. Rev. Mol. Cell Biol.*, 2008, **9**, 112–124.
48 K. Simons and W. L. C. Vaz, *Annu. Rev. Biophys. Biomol. Struct.*, 2004, **33**, 269–295.
49 R. S. Gracià, N. Bezlyepkina, R. L. Knorr, R. Lipowsky and R. Dimova, *Soft Matter*, 2010, **6**, 1472–1482.
50 I. R. Cooke, K. Kremer and M. Deserno, *Phys. Rev. E*, 2005, **72**, 011506.
51 I. R. Cooke and M. Deserno, *J. Chem. Phys.*, 2005, **123**, 224710.
52 T. Schneider and E. Stoll, *Phys. Rev. B*, 1978, **17**, 1302.
53 S. Plimpton, *J. Comp. Phys.*, 1995, **117**, 1–19.
54 W. M. Brown, P. Wang, S. J. Plimpton and A. N. Tharrington, *Comp. Phys. Comm.*, 2011, **182**, 898–911.
55 J. D. Weeks, D. Chandler and H. C. Andersen, *J. Chem. Phys.*, 1971, **54**, 5237–5247.
56 A. V. Dobrynin and J.-M. Y. Carrillo, *Macromolecules*, 2010, **44**, 140–146.
57 K. E. Norman and H. Nymeyer, *Biophys. J.*, 2006, **91**, 2046–2054.
58 T. M. Raschke, J. Tsai and M. Levitt, *Proc. Natl. Acad. Sci. U.S.A.*, 2001, **98**, 5965–5969.
59 J.-M. Y. Carrillo, J. Katsaras, B. G. Sumpter and R. Ashkar, *J. Chem. Theory Comput.*, 2017, **13**, 916–925.
60 M. Schick, *Phys. Rev. E*, 2012, **85**, 031902.
61 J. D. Nickels, X. Cheng, B. Mostofian, C. Stanley, B. Lindner, F. A. Heberle, S. Perticaroli, M. Feygenson, T. Egami, R. F. Standaert, J. C. Smith, D. A. A. Myles, M. Ohl and J. Katsaras, *J. Am. Chem. Soc.*, 2015, **137**, 15772–15780.
62 M. Hu, J. J. Briguglio and M. Deserno, *Biophys. J.*, 2012, **102**, 1403–1410.
63 H. Bermúdez, D. A. Hammer and D. E. Discher, *Langmuir*, 2004, **20**, 540–543.
64 U. Seifert, *Adv. Phys.*, 1997, **46**, 13–137.
65 S. T. Milner and S. A. Safran, *Phys. Rev. A*, 1987, **36**, 4371–4379.
66 G. Gompper and D. M. Kroll, *Phys. Rev. E*, 1995, **51**, 514–525.
67 D. H. Boal and M. Rao, *Phys. Rev. A*, 1992, **46**, 3037–3045.
68 W. Pezeshkian and J. H. Ipsen, *Soft Matter*, 2019, **15**, 9974.
69 S. J. Marrink, A. H. de Vries, T. A. Harroun, J. Katsaras and S. R. Wassall, *J. Am. Chem. Soc.*, 2008, **130**, 10–11.
70 N. Kučerka, D. Marquardt, T. A. Harroun, M.-P. Nieh, S. R. Wassall, D. H. de Jong, L. V. Schäfer, S. J. Marrink and J. Katsaras, *Biochem.*, 2010, **49**, 7485–7493.
71 K. Atkovska, J. Klingler, J. Oberwinkler, S. Keller and J. S. Hub, *ACS Cent. Sci.*, 2018, **4**, 1155–1165.

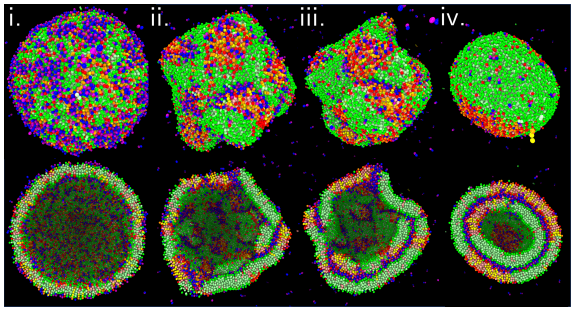

Coarse-grained models show double membrane formation from single-membrane, heterogeneous liposomes in the presence of small, hydrophobic molecules.